RSC Advances

PAPER

View Article Online
View Journal | View Issue

Cite this: *RSC Adv.*, 2020, **10**, 9985

A novel hafnium–graphite oxide catalyst for the Meerwein–Ponndorf–Verley reaction and the activation effect of the solvent†

Xiaomin Li,[a] Zhengjiang Du,[a] Yi Wu,[a] Yadong Zhen,[a] Rixin Shao,[a] Bingqi Li,[a] Chengmeng Chen,[b] Quansheng Liu[a] and Huacong Zhou *[a]

Received 22nd December 2019
Accepted 4th March 2020

DOI: 10.1039/c9ra10795a

rsc.li/rsc-advances

Construction and application of novel hydrogenation catalysts is important for the conversion of carbonyl or aldehyde compounds into alcohols in the field of biomass utilization. In this work, a novel, efficient, and easily prepared hafnium–graphite oxide (Hf–GO) catalyst was constructed *via* the coordination between Hf^{4+} and the carboxylic groups in GO. The catalyst was applied into the hydrogenation of biomass derived carbonyl compounds *via* the Meerwein–Ponndorf–Verley (MPV) reaction. The catalyst gave high efficiency under mild conditions. An interesting phenomenon was found whereby the activity of the catalyst increased gradually in the initial stage during reaction. The solvent, isopropanol, was proved to have an activation effect on the catalyst, and the activation effect varied with different alcohols and temperatures. Further characterizations showed that isopropanol played the activation effect *via* replacing the residual solvent (DMF) in micro- and mesopores during the preparation process, which was hard to be completely removed by common drying process.

Introduction

Catalytic conversion of biomass into value-added chemicals has attracted increasing attention due to the rapid depletion of fossil fuels and escalating consumption of energy.[1,2] From the viewpoint of CO_2 emission, biomass is well known as a carbon-neutral resource,[3,4] which can be converted into various chemicals, such as alcohols or hydrocarbons,[5,6] gluconic acid,[7] 5-hydroxymethylfurfural,[8–10] lactic acid,[11,12] dimethyl furan,[13] levulinic acid (LA),[14,15] and γ-valerolactone (GVL).[16–18] The hydrogenation conversion of carbonyl derivatives from biomass into alcohols or their derivatives was an important step among the reaction chains of biomass utilization. For example, levulinic acid or its esters, key platforms in biomass conversion, can be converted into the famous derivative GVL *via* hydrogenation reaction, and GVL has broad applications such as fuel additives and as a raw material for the production of valuable hydrocarbons.[19–25] Hydrogenation reactions and the corresponding catalysts were especially important for the catalytic conversion utilization of biomass. To date, various hydrogenation catalysts have been developed for the conversion of carbonyl platforms from biomass, such as palladium,[26] ruthenium,[27] platinum,[28] iridium,[29] nickel,[30] cobalt,[31] molybdenum,[32] and copper.[33] Though moderate or even high efficiency was achieved by using these catalysts, there are still some issues to be improved. One is the potential catalyst cost and metal reserves on earth for the precious metal catalysts during future large-scale applications, and thus it was still desirable to explore more potential candidates for hydrogenation reaction. On the other hand, these reported catalysts were often applied using gaseous H_2 as hydrogen sources. Generally, a relatively high H_2 pressure was often required to improve the catalytic performances of the catalysts, leading to potential safety issues in applications. Furthermore, many transition metal based catalysts often required relatively high temperatures to achieve satisfied performances, which increased the energy input and risk of accidents.

Compared to hydrogenation under H_2 atmosphere, catalytic transfer hydrogenation known as Meerwein–Ponndorf–Verley (MPV) reduction using secondary alcohols or formic acid as hydrogen source is often seen as milder hydrogenation process. Various catalysts were reported to be efficient to catalyze MPV reaction.[26–35] Among the transition metal catalysts for MPV reactions, zirconium-based catalysts were comprehensively reported giving high efficiency.[34,35] Very recently, hafnium-based catalysts were reported with higher activity and milder reaction conditions than the zirconium-based catalysts. Different organic ligands were used to prepare Hf catalysts, including porphyrins, benzoic acid, and phytate.[36–41] Up to now, the kinds of ligands being reported are still very limited and some of them

[a]*College of Chemical Engineering, Inner Mongolia University of Technology, Inner Mongolia Key Laboratory of High-Value Functional Utilization of Low Rank Carbon Resources, Hohhot 010051, Inner Mongolia, China. E-mail: hczhou@imut.edu.cn*

[b]*CAS Key Laboratory of Carbon Materials, Institute of Coal Chemistry, Chinese Academy of Sciences, China*

† Electronic supplementary information (ESI) available. See DOI: 10.1039/c9ra10795a

suffer from the high costs, inconvenience to obtain, and/or not satisfied thermal stability. Therefore, it was desirable to explore more potential materials to construct Hf based catalysts.

Besides constructing new and efficient catalysts, the effects of the solvents on catalyst activities were also important issues in catalytic conversion systems of biomass. For MPV reactions, the common solvent, isopropanol, played its role generally by acting as both solvent and hydrogen donor by donating hydrogen atoms. Among the reported catalysts for MPV reactions, more attentions were paid on the construction of novel catalysts.[26–35] However, the effects of the solvents on the activity of the catalysts were not concerned enough. Therefore, disclosing the effects of the solvents when constructing novel MPV catalysts is relatively appreciated.

In this work, graphite oxide (GO) was used to construct a novel hafnium–graphite oxide (Hf–GO) hybrid catalyst. GO was chosen due to the abundant acidic carboxylic groups and phenolic hydroxyl groups connected with aromatic structures.[42] Besides, GO is a readily purchasable and stable carbonaceous material with unique physicochemical properties and broad applications.[43–48] This study was started by the preparation of Hf–GO catalyst (Scheme 1). The catalyst was prepared simply by coordination reaction of $HfCl_4$ with commercial GO in DMF. The solvent, isopropanol, was found and proved to have an activation effect on the catalyst, and the possible reason was analyzed. As far as we know, this is the first report of constructing Hf-based catalyst using graphite oxide as the ligand for the catalytic transfer hydrogenation of ethyl levulinate and other carbonyl compounds. With the advantages of high efficiency, excellent stability, and facile preparation, the Hf–GO catalyst may have potential applications in the field of biomass conversion.

Results and discussion

Studies of the preparation conditions of catalysts

In the preparation process of the catalyst, the effects of raw material ratio, aging temperature and aging duration for Hf–GO preparation were investigated (Fig. 1). The exact content of the oxygen-containing acidic groups were complex to determine precisely. Therefore, the effect of the amount of Hf precursor ($HfCl_4$) on the catalytic activity was studied by varying the mass ratios of Hf precursor to GO. As shown in Fig. 1A, the conversion and product yield reached the highest values when the mass

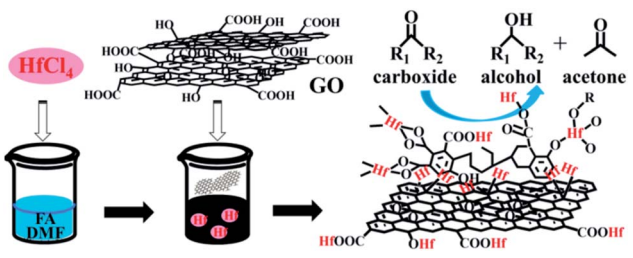

Scheme 1 Schematic illustration of the Hf–GO catalyst preparation and its application in the conversion of carbonyl compounds into alcohols.

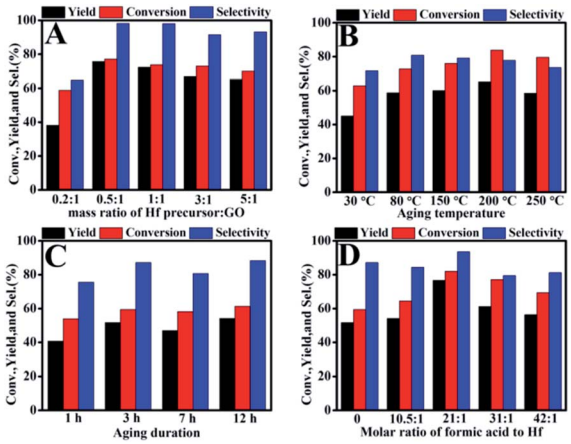

Fig. 1 Effects of preparation conditions on the performance of Hf–GO catalyst for the conversion of EL to GVL. (A) Effects of the mass ratio of Hf precursor : GO, (B) aging temperature, (C) aging duration, and (D) formic acid dosage.

ratio of Hf precursor to GO was 0.5 : 1. With further increasing the Hf precursor dosage, the GVL yield had a slight decrease. The activity of the catalyst came to the optimal values when the aging temperature and aging duration came to 80 °C and 3 h, respectively (Fig. 1B and C), and further increasing the temperature or time the yield had no significant change. Many reports employed formic acid as a modulator to facilitate the formation of the crystalline structures during the preparation of catalysts.[40,49,50] The effect of formic acid as well as other acidic modulators was studied for Hf–GO preparation, shown in Fig. 1D and Table S2.† Among the organic and inorganic acidic modulators, formic acid showed the promoting effect on the activity of the catalyst. The addition of suitable amount of formic acid could increase the activity of the catalyst, and both GVL yield (76.7%) and EL conversion (82.0%) reached the highest values when the molar ratio 21 : 1 of formic acid to Hf was used.

As seen in Fig. 1A, the mass ratio of Hf precursor to GO was the key factor influencing the activity of the catalyst, and thus we characterized the Hf–GO catalysts prepared under different raw material ratios. The textural properties of the catalysts with various mass ratios were first characterized using N_2 adsorption–desorption isotherms (Fig. S1†). The surface area and pore volume first dropped for mass ratios of Hf precursor to GO from 0.2 to 1, and then slightly increased with larger mass ratios. Compared with the surface area and pore volume, the change in average pore diameter was reversed (Table S1†). The N_2 adsorption–desorption isotherms revealed the typical mesoporous character (Fig. S1†). The Hf content in Hf–GO-0.5 : 1 was 10.01 wt%, which was higher than that of Hf–GO-0.2 : 1 (6.64 wt%) as confirmed by inductively coupled plasma atomic emission spectrometry (ICP-AES Table S1†). The Hf contents in other catalysts almost maintained constant despite further increasing the mass ratios of Hf precursor to GO. Therefore, 0.5 : 1 was selected as the optimal ratios for the preparation of Hf–GO.

The effects of the modulators were analyzed in detail (Fig. 1D and Table S2†). As seen, the GVL yield and EL conversion

reached 51.7% and 59.4% at 150 °C in 3 h without formic acid. The activity of the catalyst gradually increased with the formic acid dosage increased, and the GVL yield (76.7%) and EL conversion (82.0%) reached the highest values when the molar ratio 21 : 1 of formic acid to Hf was used. Further increasing the formic acid dosage, the activity gradually decreased. It was reported that the monocarboxylic acids were usually added in the synthesis of MOFs as modulators.[40,49–51] Seemingly, the monocarboxylic acid is not necessarily incorporated in the structure but can strongly affect the connectivity of the inorganic node by coordinates to metal ions (Hf^{4+}).[52–54] The carboxylate ligands have lower pK_a and possess stronger coordination ability, leading to the partial replacement of the modulators and the formation of structural defects.[55–63] It was also reported that the addition of formic acid could increase the acidity.[64] We also studied the effect of different modulators for Hf–GO preparation shown in Table S2.† We chose five different modulators with identical mole ratio to Hf. The results show that the catalyst using formic acid as modulator gave the highest catalytic activity.

Based on the above results, the preparation conditions were investigated, including the mass ratio of hafnium precursor ($HfCl_4$) to GO, aging temperature, aging duration, modulators and their dosage. The catalyst showed higher activity for the conversion of ethyl levulinate into GVL under the preparation conditions of the mass ratio of $HfCl_4$ to GO 0.5 : 1, aging temperature 80 °C, aging duration 3 h, formic acid as modulator with the dosage of the molar ratio of formic acid to Hf 21 : 1. The Hf–GO catalyst prepared under this condition was further characterized and studied.

Catalyst characterization

The structures of the catalyst obtained under the above optimized conditions were characterized (Fig. 2). SEM and TEM showed that Hf–GO maintained the typical dimensional sheet structures of GO (Fig. 2A and B). EDS mapping results showed that Hf element was introduced into GO successfully and dispersed on GO uniformly (Fig. 2C and D). The FTIR spectrum of GO and Hf–GO catalyst in Fig. 2E exhibited the asymmetric (GO, 1731 cm^{-1}; Hf–GO, 1723 cm^{-1}) and symmetric (GO, 1616 cm^{-1}; Hf–GO, 1655 cm^{-1}) stretching vibration of carboxylate groups. FTIR showed that the wavenumber difference of the asymmetric and symmetric vibrations of carboxylate anions was narrowed from 115 cm^{-1} for GO to 68 cm^{-1} for Hf–GO, indicating that Hf^{4+} was coordinated with carboxylate groups.[65–67] It has reported the bands at around 520 and 760 cm^{-1} were characteristic of Hf–O bonds.[68] The new absorption band at 690 cm^{-1} could be assigned to the Hf–O bond vibration (Fig. 2E).[68] As shown in XRD patterns (Fig. 2F), no obvious characteristic peaks of HfO_2 or $Hf(OH)_4$ appeared, indicating that Hf dispersed uniformly and did not form crystal aggregates. The 001 peak of GO shifted from 12° to 10°, corresponding to the layer distance enlargement from 0.74 nm to 0.80 nm, indicating that some of the Hf^{4+} were inserted into the layers of GO. The Raman spectra revealed that the G band for Hf–GO had a red shift to 1589 cm^{-1} and D band had a blue shift

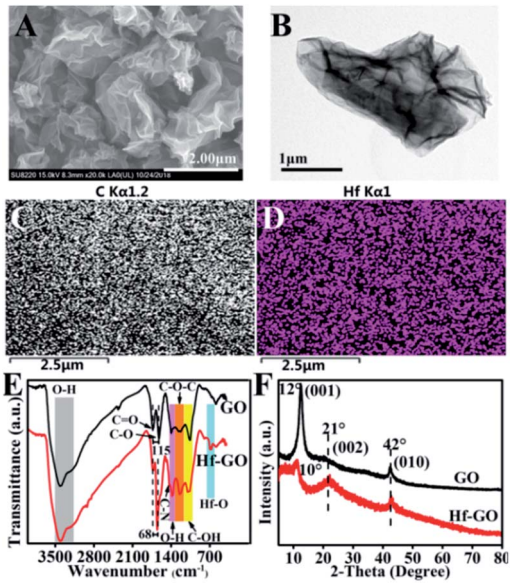

Fig. 2 (A) SEM image, (B) TEM image, (C and D) C and Hf EDS mappings of Hf–GO, (E) FTIR spectra, (F) XRD patterns of Hf–GO and GO.

to 1350 cm^{-1} as compared to GO (1596 cm^{-1}, 1345 cm^{-1}) (Fig. S2†). Furthermore, the intensity ratio of D and G peaks (I_D/I_G) increased slightly from 0.94 to 1.00 (Table S4†) after assembly of GO with Hf^{4+}. XPS full spectra, fitted spectra of Hf 4d and Hf 4f again proved the successful introduction of Hf^{4+} in Hf–GO (Fig. 3). The XPS curve-fitted spectrum revealed the Hf $4d^{5/2}$ and Hf $4d^{3/2}$, Hf $4f^{7/2}$ and Hf $4f^{5/2}$ could be detected corresponding to the hafnium–oxygen bonds at 213.8 eV and 224.4 eV, 17.4 eV and 19.1 eV, respectively (Fig. 3C and D). And these spectra were calibrated by C 1s peak at 284.8 eV. In Fig. 3B and C 1s peaks were deconvoluted into four bands based on the literatures.[69–72] The contents of C–C or C–H, C–OH or C–O–C,

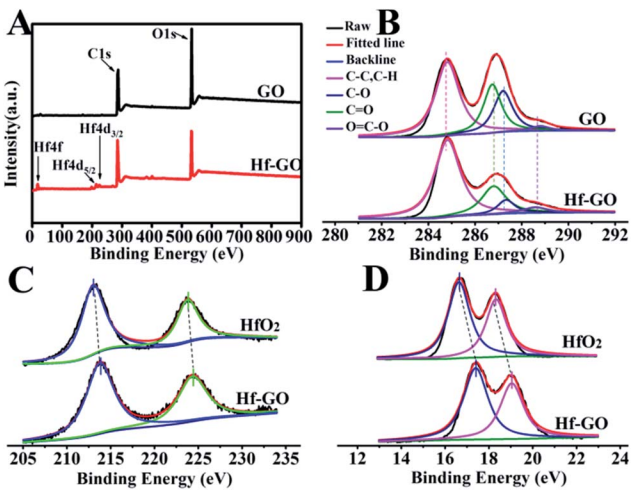

Fig. 3 (A) XPS full spectra, (B) the fitted spectra of C 1s peak of GO and Hf–GO, (C) the fitted spectra of Hf 4d, and (D) Hf 4f of HfO_2 and Hf–GO.

C=O, and O=C–O from Fig. 3B were summarized in Table S5.† The main peak at 284.8 eV originates in sp^2 (C=C), sp^3 (C–C) carbon and C–H. The deconvoluted peak centered at the binding energies of 286.7, 287.2, and 288.8 eV were considered as the C–O (hydroxyl and ethers groups), C=O (carbonyl groups), and O=C–OH (carboxyl groups) oxygen-containing carbonaceous bands, respectively. The intensity of the peak assigned to oxygen-containing carbonaceous bands of the C–O, C=O and O=C–O for GO decreased after the introduction of Hf^{4+}. These results indicated the successful covalent coordination of Hf^{4+} with COOH in GO. ICP-AES showed that the content of Hf in the catalyst was around 9.04 wt%. The results of elemental analysis of different catalysts were given in Table S6.† N_2 adsorption–desorption isotherms showed that the porous structure and the surface area, pore volume, and average pore size of the catalyst were 61.8 $m^2\ g^{-1}$, 0.08 $cm^3\ g^{-1}$, and 6.1 nm, respectively (Fig. S3C and Table S7†). TG analysis showed that the thermal stability after 300 °C of the Hf–GO catalyst was better than that of GO due to the coordination of Hf^{4+} with the carboxylic groups, and the catalyst was stable enough under reaction temperature range (<200 °C) (Fig. S3D†). The detailed discussions of catalyst characterization were given in ESI.†

Effect of reaction conditions on transfer hydrogenation

Next, the effects of the reaction conditions on transfer hydrogenation were investigated with isopropanol as the hydrogen source, including the catalyst dosage (Fig. S4A†), reaction temperature (Fig. S4B†) and reaction time (Fig. S4C†). The discussions were given in ESI.† The catalyst gave satisfied reaction results and rate under the conditions of catalyst dosage >0.05 g and reaction temperature >150 °C for the studied reaction system. The EL conversion, GVL yield, and GVL selectivity could reach to 96.5%, 88.8%, and 92.0%, respectively, under the conditions of catalyst dosage 0.1 g, reaction temperature 150 °C, and reaction time 9 h. The GVL yield did not increase when removing the solid catalyst during reaction, indicating Hf–GO was a heterogeneous catalyst (Fig. S4D†).

Comparison with other catalysts

In order to see the performances of the state-of-the-art catalyst for the MPV reaction, the performance of Hf–GO was compared various other catalysts, including Hf-, Zr-, Pd-, Ru-, Pt-, Ir-, Co-, Ni-, Mo-, and Cu-based catalysts (Table 1). The catalysts with the same reaction and similar reaction conditions were chosen and compared. The performances of around 37 kinds of catalysts were compared. When using H_2 as hydrogen source, Mo_2C/CNT (entry 37), Pd/AC (entry 21), Ni/γ-Al_2O_3 (entry 36) gave higher activities than other catalysts, with TOF values of 10.3 h^{-1} (150 °C), 7.94 h^{-1} (100 °C), and 7.67 h^{-1} (200 °C), respectively. When using isopropanol as hydrogen source, GO–Hf prepared in this work gave the highest activity with TOF values of 3.51 h^{-1} (150 °C). Among all the 37 catalysts, Hf–GO ranks basically the forth in viewpoint of TOF value. The above comparison analysis should that Hf–GO was efficient for the MPV reaction of ethyl levulinate.

Substrate scope expansion

Encouraged by the excellent performance of Hf–GO in the conversion of EL to GVL, we investigated the possibility of the MPV reactions of other carbonyl compounds with different structures (Table 2). The results showed that aliphatic and aromatic aldehydes could be effectively hydrogenated to corresponding alcohols at 70–100 °C within 2–4 h (entries 2–8). While ketones, especially with long aliphatic chains, needed a higher reaction temperature or longer reaction time of the harsh conditions to achieve satisfied conversions and yields as compared to aldehydes (entries 10 and 11). Hf–GO displayed high efficiency for cyclohexanone (conversion, yield, selectivity all >99%) (entry 9), under not yet optimized conditions. These results substantiated the universality of Hf–GO catalyst in the conversion of different carbonyl compounds with various structures.

Recycle of the Hf–GO catalyst

During the recycling process, an interesting and unexpected phenomenon was observed that the activity of Hf–GO increased with the initial 3 uses and then stabilized at a similar level without significant decreasing after 11 cycles compared to the first use (Fig. 4). The slight decreasing trend from the 6th use to the 11th use was due to the loss of the catalyst during the centrifugation recycling process. After the catalyst dosage was replenished to the initial level, the performance could be recovered (12th use). The activity increasing of Hf–GO during the initial uses draw us much attention because few reports mentioned this phenomenon for the analogue catalysts. We speculated that Hf–GO was activated by certain components in the reaction system. Mainly four components in the reaction system existed, including EL (the reactant), GVL (the product), isopropanol (the solvent), and acetone (the by-product). In order to disclose the "activator", the catalyst was pretreated by the above components, respectively, under 150 °C to simulate the reaction conditions. As shown in Fig. 5, only the pretreatment by isopropanol (Run 1 in Fig. 5A) could increase the activity of Hf–GO compared with no pretreatment (Run 0 in Fig. 5A). The pretreatment by EL, GVL, and acetone could not activate Hf–GO (Run 0 *vs.* Run 1) and the activity only increased after the first catalytic reaction (Run 2 and 3 *vs.* Run 1). Thus, it was isopropanol that played the role of activation effects. Subsequently, temperature was proved to be a key factor for the activation effect (Fig. S5†). The activation effect became more and more obvious with the increasing of temperature in the range of room temperature to 150 °C (Fig. S6†). Further increasing the pretreatment temperature led to the decreasing of the activating trend, which might be due to the gradual decomposition of the carboxylate groups under higher temperatures. Temperatures in the range of 120–150 °C were optimal activation temperature, which just fell into the optimal reaction temperature of EL to GVL.

Besides isopropanol, other alcohols were also studied to check if they had activation effects on Hf–GO (Fig. S7 and S8†). It could be seen that all the alcohols studied had activation effects on Hf–GO but the extents varied. The activation effects of the secondary alcohols were generally higher than that of the primary alcohols, with isopropanol and isobutanol giving the most significant

Table 1 MPV reaction of ethyl levulinate (EL) or levulinic acid (LA) over various catalysts under different conditions

Entry	Catalyst	Reaction conditions	EL conv. (%)	LA conv. (%)	GVL yield (%)	GVL sel. (%)	TOF[b] (h^{-1})	Ref.
1	Blank	IPA, 150 °C, 5 h	<1		0	0	—	This work
2	GO	IPA, 150 °C, 3 h	36.8		0	0	—	This work
3	Hf–GO[a]	IPA, 150 °C, 5 h	95.5		87.7	91.8	3.51	This work
4	Hf–GO[a]	IPA, 130 °C, 15 h	88.4		82.6	93.5	1.10	This work
5	Zr–GO[a]	IPA, 150 °C, 5 h	54.8		54.7	99.8	2.18	This work
6	Al–GO[a]	IPA, 150 °C, 5 h	12.2		7.5	62.0	0.3	This work
7	Cr–GO[a]	IPA, 150 °C, 5 h	3.5		0.9	25.8	0.04	This work
8	Fe–GO[a]	IPA, 150 °C, 5 h	7.1		1.3	17.7	0.05	This work
9	Cu–GO[a]	IPA, 150 °C, 5 h	5.0		1.1	23.1	0.04	This work
10	Sn–GO[a]	IPA, 150 °C, 5 h	22.3		2.4	10.6	0.10	This work
11	FDCA–Hf[c]	IPA, 160 °C, 4 h	>99		98	98	1.53	64
12	HfO_2[c]	IPA, 160 °C, 4 h	28		22	79	0.34	64
13	Zr–HA[d]	IPA, 150 °C, 11 h	99.5		84.2	84.6	0.1	65
14	Hf–ATMP[e]	IPA, 150 °C, 4 h	95		86	91	0.41	73
15	HfO_2[f]	IPA, 150 °C, 4 h	49		35	71	0.09	73
16	Hf–EDPA[g]	IPA, 150 °C, 4 h	87		74	85	0.34	73
17	Hf–MOF-808[h]	IPA, 120 °C, 8 h	NG[s]		94	NG	1.18	49
18	DUT67(Hf)[i]	IPA, 160 °C, 4 h	98.9		90.5	91.5	—	74
19	UiO-66(Hf)[j]	IPA, 160 °C, 4 h	73.9		58.5	79.1	—	74
20	PPOA–Hf[k]	IPA, 160 °C, 6 h	100		85	85	—	75
21	Pd/AC[l]	H_2 0.5 MPa, 100 °C, 5 h, H_2O	38		28	74	7.94	26
22	Co	H_2 3.3 MPa, 130 °C, 3 h	99		94	95	0.19	31
23	Zr–PhyA[m]	IPA, 150 °C, 6 h	100		96.7	96.7	0.25	35
24	Zr–RSL[n]	IPA, 160 °C, 12 h	92.4		81.1	87.8	0.48	76
25	Zr–HAs[o]	IPA, 150 °C, 15 h	>99		85.0	>85.9	0.09	34
26	Zr–HAf[p]	IPA, 150 °C, 9 h	92.7		90.1	97.2	0.09	77
27	Zr–HAt[p]	IPA, 150 °C, 7 h	92.8		92.6	99.8	0.09	77
28	Zr–SRf[p]	IPA, 150 °C, 7 h	92.4		92.0	99.6	0.43	77
29	Zr–SRt[p]	IPA, 150 °C, 9 h	95.4		92.0	96.3	0.31	77
30	Zr–HBA[q]	IPA, 150 °C, 4 h	100		94.4	94.4	—	78
31	Zr–CA[r]	IPA, 150 °C, 4 h	100		96.9	96.9	—	79
32	Ru/OMC-P	H_2 7 bar, 70 °C, 6 h, H_2O		98	92	94	1.61	27
33	Ru/carbon	H_2 1 bar, 265 °C, 50 h, H_2O		100	98.6	98.6	0.04	28
34	Pd/carbon	H_2 1 bar, 265 °C, 50 h, H_2O		100	90	90	0.04	28
35	Pt/carbon	H_2 1 bar, 265 °C, 50 h, H_2O		100	30	30	0.02	28
36	Ni/γ-Al_2O_3	H_2 50 bar, 200 °C, 4 h, H_2O		92	92	100	7.67	30
37	Mo_2C/CNT	H_2 30 bar, 150 °C, 1 h, H_2O		83	75	90.3	10.3	32
38	Cu-catalyst	H_2 70 bar, 200 °C, 10 h, H_2O		>99	91	>91	—	80
39	Ni/$MgAlO_{2.5}$	H_2 3 MPa, 160 °C, 1 h, dioxane		100	99.7	99.7	1.46	81

[a] Preparation condition: 1 mL formic acid was dissolved in DMF (400 mL), 1.59 mmol metal chloride was added into DMF solution with continuously stirred and completely dissolved. After that, 1.0 g of GO was directly added to the $HfCl_4$ solution and the obtained mixture was stirred for 3 h at 30 °C, then aged at 80 °C under static conditions for 3 h. The suspended solution was separated by filtration to give black precipitate, and successively washed with DMF, ethanol for 4 times, dried under vacuum conditions at 80 °C for 24 h, and crowded into powders. Reaction conditions: 1 mmol EL, 0.1 g catalyst (5 mol% Hf), 5 mL 2-PrOH. [b] TOF (turnover frequency) = (mole of GVL)/(mole of active metal × reaction time). [c] Data obtained from ref. 64, FDCA: furan dicarboxylic acid, 16 mol% Hf. [d] Data obtained from ref. 65, HA: humic acid. [e] Data obtained from ref. 73, the mole of Hf was 52 mol%. [f] Data obtained from ref. 73, 95 mol% Hf. [g] Data obtained from ref. 73, 54 mol% Hf (ICP determined). [h] Data obtained from ref. 49, MOF-808: 1,3,5-benzenetricarboxylic acid, 10 mol% Hf. [i] Data obtained from ref. 74, DUT67: 2,5-thiophenedicarboxylic acid. [j] Data obtained from ref. 74, UiO-66: terephthalic acid. [k] Data obtained from ref. 75, PPOA: phenylphosphonic acid. [l] AC: active carbon. [m] PhyA: phytic acid. [n] RSL: raw Shengli lignite. [o] HAs: humic acids. [p] Humic acids (HA) extracted from lignite and the solid residues (SR). [q] HBA: 4-hydroxybenzoic acid dipotassium salt. [r] CA: cyanuric acid. [s] NG: not given.

activation effect. Other solvents such as decane, acetone, and 2-hexanone were also used to pretreat Hf–GO, and it was found that these solvents could not activate the catalyst (Fig. S9†). The reasons for this would be discussed below.

Characterization of the recycled and captivated Hf–GO

The intrinsic mechanism for the activation effect of alcohols was analyzed by characterizing the fresh and pretreated/used Hf–GO catalysts using various techniques, including XPS, elemental analysis, XRD, Raman, TG analysis, and N_2 adsorption–desorption. No significant morphology changes and Hf chemical state changes were found for the pretreated and recycled Hf–GO (Fig. S10–S13†). The N contents decreased after solvent pretreatment except for pretreatment by DMF (Table S6†). TG analysis also showed that the weight losses of Hf–GO pretreated by solvents were much lower than that of the fresh

Table 2 MPV reduction of different biomass-derived carbonyl compounds over the Hf–GO catalyst[a]

Entry	Substrate	Product	T (°C)	T (h)	Conv. (%)	Yield (%)	Sel. (%)
1	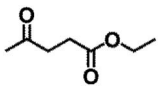	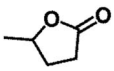	150	9	96.5	88.8	92.0
2		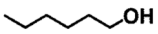	100	3	95.9	87.8	91.5
3	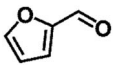	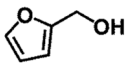	70	4	89.7	85.5	95.4
4	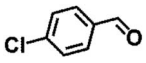	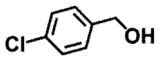	90	3	97.9	95.9	98.0
5	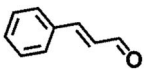	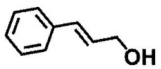	100	3	89.7	81.0	90.3
6	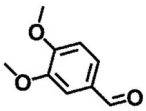	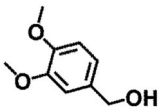	80	3	93.0	91.7	98.6
7	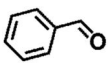	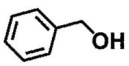	90	2	96.4	87.2	90.5
8	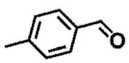	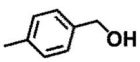	80	4	93.7	88.7	94.6
9		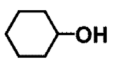	100	5	>99	>99	>99
10	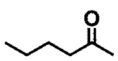	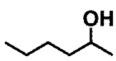	150	8	>99	>99	>99
11	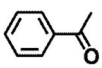	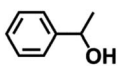	120	7	99.3	98.8	99.5

[a] Reaction conditions: substrate 1 mmol, isopropanol 5 mL, and Hf–GO 0.1 g (5 mol% Hf).

Hf–GO (Fig. S14†). FTIR showed that The C–N stretching vibration at 1424 cm^{-1} of DMF was obvious for fresh Hf–GO,[82] but it was found to be weakened after solvent treatment (Fig. S15†). Base on the above analysis, it could be deduced that solvent pretreatment removed residual DMF in Hf–GO. The residual DMF in the pore structures of Hf–GO was hard to remove even washed by ethanol and then dried under vacuum and 150 °C (boiling point of DMF under standard atmosphere) (Table S6,† entry 9). As shown in Table S6,† the N content in GO was only 0.04 wt%, but it increased to 1.55 wt% for fresh Hf–GO. The N content decreased to different extents after pretreatment by different solvents (except for Hf–GO pretreated by DMF), indicating the solvent pretreatment could indeed remove DMF residual in the catalyst. The Hf content had no significant changes, and the changes of C, H, and O contents could be attributed to the removal of DMF. It should be noted that the pretreatment by decane and acetone could also remove DMF (Table S6†), but these solvents could not activate the catalyst only if Hf–GO was allowed to contact with isopropanol (as mentioned above, Fig. S9†). Therefore, the structures of the pretreated Hf–GO were further characterized by BET and pore structure analysis (Fig. 6 and Table S7†). It could be seen that the surface area, the volumes of total pores and mesopores of Hf–GO–decane and Hf–GO–acetone were all much lower than those of Hf–GO–isopropanol, which may result in no obvious activation effect for these solvents. Isopropanol pretreatment mainly affected the structures of micro- and mesopores, indicating DMF in these pore structures was removed (Fig. 6A and B). Another possible reason was that although these solvents

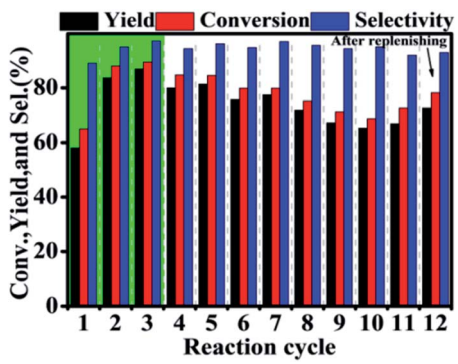

Fig. 4 Recycle of the Hf–GO catalyst. Reaction conditions: 1 mmol EL, 0.1 g catalyst (5 mol% Hf), 5 mL 2-PrOH, 150 °C, 2 h.

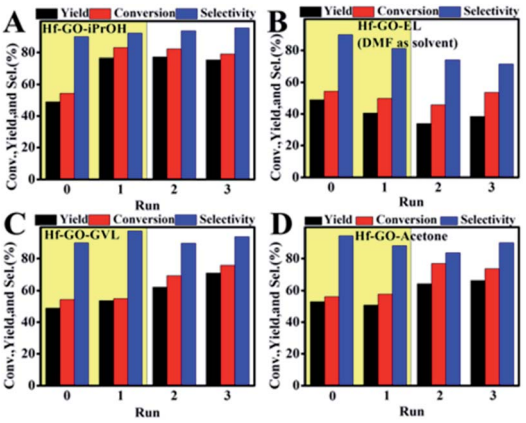

Fig. 5 Performance of the Hf–GO–X catalyst (Hf–GO pretreated by solvent X). (A) X = iPrOH; (B) X = ethyl levulinate (EL); (C) X = GVL; (D) X = acetone. Run 0: the performance of the fresh Hf–GO catalyst without pretreatment. Run 1, 2 and 3: the performance of the Hf–GO–X catalyst for subsequent three times use.

could remove DMF in mesopores of Hf–GO, they could not interact with the active Hf–O sites and provide hydrogen to promote the occurrence of the reaction. The surface contents of Hf in Hf–GO pretreated by different solvents were analyzed by XPS, and no obvious difference were observed (Table S8†). The influence of mass transfer on the performance of the catalysts were detected by prolonging the reaction time, and both conversion and yield for Hf–GO–iPrOH were higher than those for Hf–GO-fresh throughout the whole time range, further indicating isopropanol pretreatment had an activation effects on Hf–GO (Fig. S16†). In conclusion, it could be postulated that isopropanol played its activation effects on Hf–GO by first replacing DMF in micro- and mesopores and then interacting with active Hf–O sites to promote the proceeding of the reaction.

Besides Hf–GO catalyst, the above discussed activation effects of isopropanol also existed for Zr–GO catalyst, but was not obvious for Hf–H_3BTC constructed by 1.3.5-benzene tricarboxylic acid (Fig. S17†). This was related to the different pore structures of the catalysts (Fig. 6 and S18†). Hf–GO had obvious micro- and mesoporous structures. For Hf–H_3BTC, there were abundant pores larger than 10 nm and the distribution of pore diameters were broad, leading to the easy removal of DMF during preparation by washing and much less DMF residue in the catalyst compared to Hf–GO (Fig. 6C and D and Table S6†). Therefore, isopropanol could easily contact with the active sites in the first use, and no obvious increasing of activity was observed during the subsequent use. Comparatively, Hf–GO had abundant micro- and mesopores (Fig. 6A and B), leading to the residue of DMF, and thus isopropanol could activate the catalyst *via* removing DMF as discussed above.

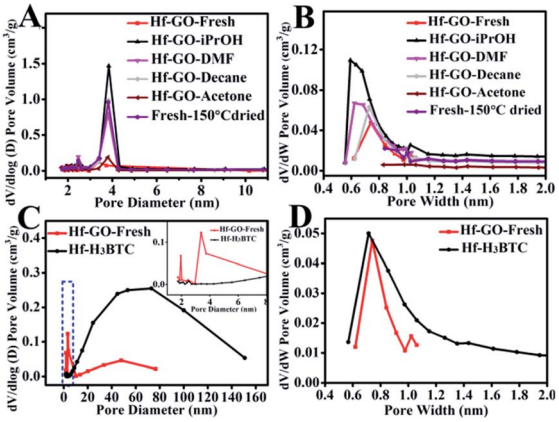

Fig. 6 Mesopore distributions of different catalysts (A and C) and micropore distributions of different catalysts (B and D). The mesopore size distribution was calculated based on the DFT method. The micropore size distribution was calculated based on the H–K method.

Experimental

Materials

Ethyl levulinate (EL, 98%), γ-valerolactone (GVL, 98%), zircomiun tetrachloride ($ZrCl_4$, 98%), 1,3,5-benzenetricarboxylic acid (H_3BTC, 99%), furfural (FF, 99%) and furfuryl alcohol (FA, 98%) were provided by J&K Scientific Ltd. Hafnium tetrachloride ($HfCl_4$, 98+%) and chromium(III) chloride anhydrous ($CrCl_3$, 98%) were obtained from Alfa. Aluminum chloride ($AlCl_3$, 99%), iron chloride ($FeCl_3$, ≥99.9%), copper chloride ($CuCl_2$, 98%) and tin chloride ($SnCl_4$, AR) were provided by Aladdin Industrial Corporation. Graphite oxide (GO) were provided by Institute of Coal Chemistry, Chinese Academy of Sciences. Isopropanol (iPrOH, 99.9%) was provided by Innochem. *N*,*N*-Dimethylformamide (DMF, >99.9%), *n*-butanol (*n*BuOH, ≥99.7%), *n*-propanol (*n*PrOH, ≥99.9%), isobutanol (sBuOH, ≥99.5%), methanol (MeOH, ≥99.9%), ethanol (EtOH, 100%), 1-hexanol (*n*HeOH, >99.5%), *n*-octanol (*n*OcOH, ≥99%) and 2-hexanol (sHeOH, 99%) were provided by Aladdin Industrial Corporation. Decane (AR) and other chemicals were obtained from Beijing Institute of Chemical Reagent.

Preparation of different M–GO catalysts

The M–GO catalysts (M = Hf, Zr, Al, Cr, Fe, Cu, Sn) were obtained by the simple synthesis of GO with an equivalent mole of metal chloride (*i.e.*, $HfCl_4$, $ZrCl_4$, $AlCl_3$, $CrCl_3$, $FeCl_3$, $CuCl_2$ or $SnCl_4$) and 0–2.0 mL of formic acid in DMF under stirring conditions. In a typical preparation process for Hf–GO, 1.359 g (1 mL) formic acid (FA) was dissolved in DMF (400 mL), 0.5 g $HfCl_4$ was added into DMF solution with continuously stirred and completely dissolved. After that, 1.0 g of GO was directly added to the $HfCl_4$ solution and the obtained mixture was stirred for 3 h at 30 °C, then aged at 80 °C under static conditions for 3 h. The suspended solution was separated by filtration to give black precipitate, and successively washed with DMF, ethanol for 4 times, dried under vacuum conditions at 80 °C for 24 h, and crowded into powders for use. For comparison, the Hf–H_3BTC organic–inorganic hybrid was prepared by solvothermal treatment of $HfCl_4$ and equimolecular 1,3,5-benzenetricarboxylic acid in DMF at 120 °C under static conditions for 48 h, referencing to a previously reported synthetic

methods.[51,83] All the solid samples were after dried at 80 °C for 4 h for the catalyst characterization and analysis of catalytic performance.

The preparation parameters were studied, including effects of the mass ratio of Hf precursor: GO, aging temperature, aging duration, and formic acid dosage. The details were described as follows. (1) Effects of the mass ratio of Hf precursor to GO: 1 mL formic acid was dissolved in DMF (400 mL, five copies), $HfCl_4$ of 0.2 g, 0.5 g, 1.0 g, 3.0 g, 5.0 g, respectively, was added into DMF solution with continuously stirred and completely dissolved. After that, 1.0 g of GO was directly added to the $HfCl_4$ solution and the obtained mixture was stirred for 3 h at 30 °C, then aged at 80 °C under static conditions for 3 h. The suspended solution was separated by filtration to give black precipitate, and successively washed with DMF, ethanol for 4 times, dried under vacuum conditions at 80 °C for 24 h, and crowded into powders. (2) Aging temperature: 1 mL formic acid was dissolved in DMF (400 mL), 0.5 g $HfCl_4$ was added into DMF solution with continuously stirred and completely dissolved. After that, 1.0 g of GO was directly added to the $HfCl_4$ solution and the obtained mixture was stirred for 3 h at 30 °C, then aged at the required temperature under static conditions for 3 h. The suspended solution was separated by filtration to give black precipitate, and successively washed with DMF, ethanol for 4 times, dried under vacuum conditions at 80 °C for 24 h, and crowded into powders. (3) Aging duration: 1 mL formic acid was dissolved in DMF (400 mL), 0.5 g $HfCl_4$ was added into DMF solution with continuously stirred and completely dissolved. After that, 1.0 g of GO was directly added to the $HfCl_4$ solution and the obtained mixture was stirred for 3 h at 30 °C, then aged at 80 °C under static conditions for the required duration. The suspended solution was separated by filtration to give black precipitate, and successively washed with DMF, ethanol for 4 times, dried under vacuum conditions at 80 °C for 24 h, and crowded into powders. (4) Formic acid dosage: formic acid of 0 mL, 0.5 mL, 1.0 mL, 1.5 mL, 2.0 mL, respectively, was dissolved in DMF (400 mL, five copies), 0.5 g $HfCl_4$ was added into DMF solution with continuously stirred and completely dissolved. After that, 1.0 g of GO was directly added to the $HfCl_4$ solution and the obtained mixture was stirred for 3 h at 30 °C, then aged at 80 °C under static conditions for 3 h. The suspended solution was separated by filtration to give black precipitate, and successively washed with DMF, ethanol for 4 times, dried under vacuum conditions at 80 °C for 24 h, and crowded into powders. Reaction conditions: 1 mmol EL, 0.1 g catalyst, 5 mL 2-PrOH, reaction temperature 150 °C, and reaction time 3 h.

The as-obtained Hf–GO was treated with different organic solvents at 150 °C for 2 h to give Hf–GO–X (X = DMF, EL, GVL, iPrOH, other various alcohols, acetone, 2-hexanone, decane). 0.1 g of the fresh catalyst was stirred in the different organic solvents at 150 °C for 2 h, recovered by centrifugation, and washed three times with fresh isopropanol to give Hf–GO–X. For the effects of pretreating temperatures in isopropanol, the fresh Hf–GO was treated with isopropanol at various temperatures for 2 h to give Hf–GO-*Y* (*Y* = 25, 50, 70, 100, 120, 150, 170, 200 °C).

Catalyst characterization

Scanning electron microscopy (SEM) measurements were performed using a Hitachi SU8220 scanning electron microscope operated at 20 kV with an energy dispersive spectrometer (EDS) apparatus. Transmission electron microscopy (TEM) images were obtained using a TEM JEM-2010 with an accelerating voltage of 120 kV. The samples were dispersed in absolute ethanol, and the suspension was sonicated for 15 min to make the sample disperse well. Then the sample solution was dropped onto the copper network containing the carbon support film, and was allowed to volatilize at room temperature for 2 h to be tested. Fourier transform-infrared spectra (FTIR) were obtained using a PerkinElmer spectrometer. X-ray diffraction (XRD) was carried out *via* an Produce-Rigaku SmartLab 9 KW X-ray diffractometer with a Cu target configuration and a highly sensitive D/teX Ultra 250 inspection system at 20° per minute ranging from 5° to 90°. The tube voltage was 45 kW, and the current was 200 mA. Raman spectrum was collected on a Renishaw® inVia microscope in the range of 120 cm^{-1} to 4000 cm^{-1} with 532 nm laser for excitation with power of 0.3 mW, 50× objective, data acquisition time 3 s, and scanning 50 cycles for each spectrum. The thermogravimetric (TG) analysis of Hf–GO was performed using a thermogravimetric analysis system (Diamond TG/DTA6300, PerkinElmer Instruments) under an N_2 atmosphere at the heating rate of 10 °C min^{-1}. The surface area and pore diameters and pore volumes were determined *via* the nitrogen adsorption–desorption method using an American Mike Micromeritics ASAP 2020 sorption analyzer. The XPS measurements were carried out *via* an ESCALAB 250Xi spectrometer (Thermo Fisher Scientific) at a pressure of $\sim 3 \times 10^{-9}$ mbar using Al Kα as the excitation source ($h\nu$ = 1486.6 eV) and operating at 15 kV and 150 W, and C 1s orbital (284.8 eV) was used to correct the binding energy. The XPSpeak 4.1 software was used to perform manual peak splitting, establishing a baseline and add peaks, adjust parameters such as peak area and half-peak width to make the fitted data coincide with the original data, keep the Lorentzian–Gaussian ratio consistent (default 80). C 1s peaks were deconvoluted into four bands.[69–72] Hf fitted spectra in which the peak area ratio was fixed ($d^{5/2} : d^{3/2} = 3 : 2$, $f^{7/2} : f^{5/2} = 4 : 3$) and the half-peak width was kept consistent. Inductively coupled plasma atomic emission spectroscopy (ICP-AES) using a Agilent 720 system. Elemental analysis (EA) using a Thermo Fisher Flash 2000 system.

The hydrogenation reduction reactions

The hydrogenation reduction of various aldehydes and ketones using isopropanol as the solvent and hydrogen-donor was performed in a 10 mL Teflon-lined stainless steel autoclave equipped with a magnetic stirrer. In a typical reaction procedure, EL or other carbonyl compounds (1 mmol), isopropanol (5 mL) and the catalyst (100 mg) were added into the reactor and tightly sealed, then placed into a preheated oil-bath at a known temperature of 130–170 °C for a reaction time of 1–9 h. After reaction, the reactor was cooled in cold water to quench the reaction and the organic phase was diluted by isopropanol. The liquid samples were analyzed quantitatively by gas

chromatography (TECHCOMP GC7900) using decane as the internal standard, and identification of the products was done by GC-MS (SHIMADZU-QP 2010).

Catalyst recycle and heterogeneity

In the experiments to investigate the reusability of the Hf–GO catalyst, the catalyst was recovered by centrifugation, washed three times with fresh isopropanol, and then the catalyst was directly used for the next run of reaction. For heterogeneity, the solid catalyst was separated from the reaction mixture by centrifugation and the supernatant was allowed to react to determine if the product yield further increased in the absence of the solid catalyst.

Conclusions

In summary, a novel and efficient Hf–GO catalyst was constructed using graphite oxide as the ligand for MPV reaction of carbonyl compounds. Both the preparation conditions and the reaction conditions were systematically studied. The prepared Hf–GO catalyst showed similar or even higher efficiency among the analogues. It was found that isopropanol had an activation effect on the catalyst by first removing residual DMF in micro- and mesopores and then interacting with the active Hf–O sites. With the advantages of good efficiency, excellent stability, and facility to prepare, the novel Hf–GO catalyst was promising in biomass conversion.

Conflicts of interest

There are no conflicts to declare.

Acknowledgements

This work was supported by the National Natural Science Foundation of China (21968021, 21606134, and 21566029), CAS "Light of West China" Program, and the Innovative and Entrepreneurial Talents Grassland Talents Engineering of Inner Mongolia.

Notes and references

1 M. Besson, P. Gallezot and C. Pinel, *Chem. Rev.*, 2014, **114**, 1827–1870.
2 D. M. Alonso, J. Q. Bond and J. A. Dumesic, *Green Chem.*, 2010, **12**, 1493–1513.
3 Q. Xu, X. L. Li, T. Pan, C. G. Yu, J. Deng, Q. X. Guo and Y. Fu, *Green Chem.*, 2016, **18**, 1287–1294.
4 H. L. Wang, Y. Q. Pu, A. Ragauskas and B. Yang, *Bioresour. Technol.*, 2019, **271**, 449–461.
5 A. Q. Wang and T. Zhang, *Acc. Chem. Res.*, 2013, **46**, 1377–1386.
6 H. L. Wang, H. M. Wang, E. Kuhn, M. P. Tucker and B. Yang, *ChemSusChem*, 2018, **11**, 285–291.
7 S. Wang, J. Wang, Q. F. Zhao, D. D. Li, J. Q. Wang, M. Cho, H. Cho, O. Terasaki, S. J. Chen and Y. Wan, *ACS Catal.*, 2015, **5**, 797–802.
8 M. Dashtban, A. Gilbert and P. Fatehi, *RSC Adv.*, 2014, **4**, 2037–2050.
9 M. E. Zakrzewska, E. Bogel-Lukasik and R. Bogel-Lukasik, *Chem. Rev.*, 2011, **111**, 397–417.
10 H. M. Mirzaei and B. Karimi, *Green Chem.*, 2016, **18**, 2282–2286.
11 Z. C. Tang, W. P. Deng, Y. L. Wang, E. Z. Zhu, X. Y. Wan, Q. H. Zhang and Y. Wang, *ChemSusChem*, 2014, **7**, 1557–1567.
12 D. Esposito and M. Antonietti, *ChemSusChem*, 2013, **6**, 989–992.
13 G. H. Wang, J. Hilgert, F. H. Richter, F. Wang, H. J. Bongard, B. Spliethoff, C. Weidenthaler and F. Schuth, *Nat. Mater.*, 2014, **13**, 294–301.
14 A. Szabolcs, M. Molnar, G. Dibo and L. T. Mika, *Green Chem.*, 2013, **15**, 439–445.
15 F. D. Pileidis and M. M. Titirici, *ChemSusChem*, 2016, **9**, 562–582.
16 J. Yuan, S. S. Li, L. Yu, Y. M. Liu, Y. Cao, H. Y. He and K. N. Fan, *Energy Environ. Sci.*, 2013, **6**, 3308–3313.
17 L. Deng, J. Li, D. M. Lai, Y. Fu and Q. X. Guo, *Angew. Chem., Int. Ed.*, 2009, **48**, 6529–6532.
18 S. H. Zhu, Y. F. Xue, J. Guo, Y. L. Cen, J. G. Wang and W. B. Fan, *ACS Catal.*, 2016, **6**, 2035–2042.
19 K. Yan, Y. Y. Yang, J. J. Chai and Y. Lu, *Appl. Catal., B*, 2015, **179**, 292–304.
20 D. M. Alonso, S. G. Wettstein and J. A. Dumesic, *Green Chem.*, 2013, **15**, 584–595.
21 J. Q. Bond, D. M. Alonso, D. Wang, R. M. West and J. A. Dumesic, *Science*, 2010, **327**, 1110–1114.
22 J. N. Chheda, G. W. Huber and J. A. Dumesic, *Angew. Chem., Int. Ed.*, 2007, **46**, 7164–7183.
23 J. P. Lange, R. Price, P. M. Ayoub, J. Louis, L. Petrus, L. Clarke and H. Gosselink, *Angew. Chem., Int. Ed.*, 2010, **49**, 4479–4483.
24 M. G. Al-Shaal, A. Dzierbinski and R. Palkovits, *Green Chem.*, 2014, **16**, 1358–1364.
25 L. Xin, Z. Y. Zhang, J. Qi, D. J. Chadderdon, Y. Qiu, K. M. Warsko and W. Z. Li, *ChemSusChem*, 2013, **6**, 674–686.
26 F. Y. Ye, D. M. Zhang, T. Xue, Y. M. Wang and Y. J. Guan, *Green Chem.*, 2014, **16**, 3951–3957.
27 A. Villa, M. Schiavoni, C. E. Chan-Thaw, P. F. Fulvio, R. T. Mayes, S. Dai, K. L. More, G. M. Veith and L. Prati, *ChemSusChem*, 2015, **8**, 2520–2528.
28 P. P. Upare, J. M. Lee, D. W. Hwang, S. B. Halligudi, Y. K. Hwang and J. S. Chang, *J. Ind. Eng. Chem.*, 2011, **17**, 287–292.
29 W. Li, J. H. Xie, H. Lin and Q. L. Zhou, *Green Chem.*, 2012, **14**, 2388–2390.
30 K. Hengst, M. Schubert, H. W. P. Carvalho, C. B. Lu, W. Kleist and J. D. Grunwaldt, *Appl. Catal., A*, 2015, **502**, 18–26.
31 H. C. Zhou, J. L. Song, H. L. Fan, B. B. Zhang, Y. Y. Yang, J. Y. Hu, Q. G. Zhu and B. X. Han, *Green Chem.*, 2014, **16**, 3870–3875.
32 E. F. Mai, M. A. Machado, T. E. Davies, J. A. Lopez-Sanchez and V. T. da Silva, *Green Chem.*, 2014, **16**, 4092–4097.

33 Y. Y. Liu, P. Ghimire and M. Jaroniec, *J. Colloid Interface Sci.*, 2019, **535**, 122–132.
34 Y. F. Sha, Z. H. Xiao, H. C. Zhou, K. L. Yang, Y. M. Song, N. Li, R. X. He, K. D. Zhi and Q. S. Liu, *Green Chem.*, 2017, **19**, 4829–4837.
35 J. L. Song, B. W. Zhou, H. C. Zhou, L. Q. Wu, Q. L. Meng, Z. M. Liu and B. X. Han, *Angew. Chem., Int. Ed. Engl.*, 2015, **54**, 9399–9403.
36 M. H. Beyzavi, N. A. Vermeulen, A. J. Howarth, S. Tussupbayev, A. B. League, N. M. Schweitzer, J. R. Gallagher, A. E. Platero-Prats, N. Hafezi, A. A. Sarjeant, J. T. Miller, K. W. Chapman, J. F. Stoddart, C. J. Cramer, J. T. Hupp and O. K. Farha, *J. Am. Chem. Soc.*, 2015, **137**, 13624–13631.
37 J. Zheng, M. Y. Wu, F. L. Jiang, W. P. Su and M. C. Hong, *Chem. Sci.*, 2015, **6**, 3466–3470.
38 M. H. Beyzavi, N. A. Vermeulen, A. J. Howarth, S. Tussupbayev, A. B. League, N. M. Schweitzer, J. R. Gallagher, A. E. Platero-Prats, N. Hafezi, A. A. Sarjeant, J. T. Miller, K. W. Chapman, J. F. Stoddart, C. J. Cramer, J. T. Hupp and O. K. Farha, *J. Am. Chem. Soc.*, 2016, **138**, 3251.
39 X. X. Cai, J. P. Pan, G. M. Tu, Y. H. Fu, F. M. Zhang and W. D. Zhu, *Catal. Commun.*, 2018, **113**, 23–26.
40 S. Rojas-Buzo, P. García-García and A. Corma, *Green Chem.*, 2018, **20**, 3081–3091.
41 J. L. Song, Z. M. Xue, C. Xie, H. R. Wu, S. S. Liu, L. Zhang and B. X. Han, *ChemCatChem*, 2018, **10**, 725–730.
42 A. K. Geim and K. S. Novoselov, *Nat. Mater.*, 2007, **6**, 183–191.
43 H. J. Shin, K. K. Kim, A. Benayad, S. M. Yoon, H. K. Park, I. S. Jung, M. H. Jin, H. K. Jeong, J. M. Kim, J. Y. Choi and Y. H. Lee, *Adv. Funct. Mater.*, 2009, **19**, 1987–1992.
44 S. Stankovich, D. A. Dikin, R. D. Piner, K. A. Kohlhaas, A. Kleinhammes, Y. Jia, Y. Wu, S. T. Nguyen and R. S. Ruoff, *Carbon*, 2007, **45**, 1558–1565.
45 H. A. Becerril, J. Mao, Z. Liu, R. M. Stoltenberg, Z. Bao and Y. Chen, *ACS Nano*, 2008, **2**, 463–470.
46 H. L. Zhou, Y. C. Liu, L. Zhang, H. D. Li, H. Liu and W. J. Li, *J. Colloid Interface Sci.*, 2019, **533**, 287–296.
47 O. Metin, H. Can, K. Sendil and M. S. Gultekin, *J. Colloid Interface Sci.*, 2017, **498**, 378–386.
48 M. Nasrollahzadeh, S. M. Sajadi, A. Rostami-Vartooni, M. Alizadeh and M. Bagherzadeh, *J. Colloid Interface Sci.*, 2016, **466**, 360–368.
49 S. Rojas-Buzo, P. Garcia-Garcia and A. Corma, *ChemSusChem*, 2018, **11**, 432–438.
50 Z. Hu, I. Castano, S. Wang, Y. Wang, Y. Peng, Y. Qian, C. Chi, X. Wang and D. Zhao, *Cryst. Growth Des.*, 2016, **16**, 2295–2301.
51 A. H. Valekar, K.-H. Cho, S. K. Chitale, D.-Y. Hong, G.-Y. Cha, U. H. Lee, D. W. Hwang, C. Serre, J.-S. Chang and Y. K. Hwang, *Green Chem.*, 2016, **18**, 4542–4552.
52 H. Reinsch, B. Bueken, F. Vermoortele, I. Stassen, A. Lieb, K.-P. Lillerud and D. De Vos, *CrystEngComm*, 2015, **17**, 4070–4074.
53 V. Bon, V. Senkovskyy, I. Senkovska and S. Kaskel, *Chem. Commun.*, 2012, **48**, 8407–8409.
54 V. Bon, I. Senkovska, I. A. Baburin and S. Kaskel, *Cryst. Growth Des.*, 2013, **13**, 1231–1237.
55 G. R. Cai and H. L. Jiang, *Angew. Chem., Int. Ed.*, 2017, **56**, 563–567.
56 H. Reinsch, B. Bueken, F. Vermoortele, I. Stassen, A. Lieb, K. P. Lillerud and D. De Vos, *Crystengcomm*, 2015, **17**, 4070–4074.
57 Z. G. Hu, I. Castano, S. N. Wang, Y. X. Wang, Y. W. Peng, Y. H. Qan, C. L. Chi, X. R. Wang and D. Zhao, *Cryst. Growth Des.*, 2016, **16**, 2295–2301.
58 H. Wu, Y. S. Chua, V. Krungleviciute, M. Tyagi, P. Chen, T. Yildirim and W. Zhou, *J. Am. Chem. Soc.*, 2013, **135**, 10525–10532.
59 F. Vermoortele, B. Bueken, G. Le Bars, B. Van de Voorde, M. Vandichel, K. Houthoofd, A. Vimont, M. Daturi, M. Waroquier, V. Van Speybroeck, C. Kirschhock and D. E. De Vos, *J. Am. Chem. Soc.*, 2013, **135**, 11465–11468.
60 Z. L. Fang, B. Bueken, D. E. De Vos and R. A. Fischer, *Angew. Chem., Int. Ed.*, 2015, **54**, 7234–7254.
61 C. A. Trickett, K. J. Gagnon, S. Lee, F. Gandara, H. B. Burgi and O. M. Yaghi, *Angew. Chem., Int. Ed.*, 2015, **54**, 11162–11167.
62 K. M. Choi, H. J. Jeon, J. K. Kang and O. M. Yaghi, *J. Am. Chem. Soc.*, 2011, **133**, 11920–11923.
63 S. He, Y. F. Chen, Z. C. Zhang, B. Ni, W. He and X. Wang, *Chem. Sci.*, 2016, **7**, 7101–7105.
64 H. Li, T. Yang and Z. Fang, *Appl. Catal., B*, 2018, **227**, 79–89.
65 Z. H. Xiao, H. C. Zhou, J. M. Hao, H. L. Hong, Y. M. Song, R. X. He, K. D. Zhi and Q. S. Liu, *Fuel*, 2017, **193**, 322–330.
66 J. L. Song, L. Q. Wu, B. W. Zhou, H. C. Zhou, H. L. Fan, Y. Y. Yang, Q. L. Meng and B. X. Han, *Green Chem.*, 2015, **17**, 1626–1632.
67 L. Peng, J. L. Zhang, J. S. Li, B. X. Han, Z. M. Xue and G. Y. Yang, *Chem. Commun.*, 2012, **48**, 8688–8690.
68 H. Li, Y. Li, Z. Fang and R. L. Smith, *Catal. Today*, 2019, **319**, 84–92.
69 G. Lv, H. Wang, Y. Yang, T. Deng, C. Chen, Y. Zhu and X. Hou, *ACS Catal.*, 2015, **5**, 5636–5646.
70 P. P. Upare, J.-W. Yoon, M. Y. Kim, H.-Y. Kang, D. W. Hwang, Y. K. Hwang, H. H. Kung and J.-S. Chang, *Green Chem.*, 2013, **15**, 2935.
71 Y. Wang, Z. M. Rong, Y. Wang, T. Wang, Q. Q. Du, Y. Wang and J. Qu, *ACS Sustainable Chem. Eng.*, 2016, **5**, 1538–1548.
72 O. Akhavan, *ACS Nano*, 2010, **4**, 4174–4180.
73 C. Xie, J. L. Song, B. W. Zhou, J. Y. Hu, Z. R. Zhang, P. Zhang, Z. Jiang and B. X. Han, *ACS Sustainable Chem. Eng.*, 2016, **4**, 6231–6236.
74 Z. Cai, W. K. Li, F. M. Wang and X. B. Zhang, *J. Taiwan Inst. Chem. Eng.*, 2018, **93**, 374–378.
75 W. B. Wu, Y. Li, H. Li, W. F. Zhao and S. Yang, *Catalysts*, 2018, **8**, 264.
76 J. X. Hao, L. M. Han, Y. F. Sha, X. X. Yu, H. Y. Liu, X. Y. Ma, Y. Z. Yang, H. C. Zhou and Q. S. Liu, *Fuel*, 2019, **239**, 1304–1314.
77 B. B. Zhang, J. X. Hao, Y. F. Sha, H. C. Zhou, K. L. Yang, Y. M. Song, Y. P. Ban, R. X. He and Q. S. Liu, *Fuel*, 2018, **217**, 122–130.

78 J. L. Song, L. Q. Wu, B. W. Zhou, H. C. Zhou, H. L. Fan, Y. Y. Yang, Q. Meng and B. X. Han, *Green Chem.*, 2015, **17**, 1626–1632.
79 Z. M. Xue, J. Y. Jiang, G. F. Li, W. C. Zhao, J. F. Wang and T. C. Mu, *Catal. Sci. Technol.*, 2016, **6**, 5374–5379.
80 K. Yan, J. Y. Liao, X. Wu and X. M. Xie, *RSC Adv.*, 2013, **3**, 3853–3856.
81 K. Jiang, D. Sheng, Z. H. Zhang, J. Fu, Z. Y. Hou and X. Y. Liu, *Catal. Today*, 2016, **274**, 55–59.
82 J. Cheng, J. Wang, X. Z. Wang and H. Wang, *Ceram. Int.*, 2017, **43**, 7159–7165.
83 H. Furukawa, F. Gandara, Y. B. Zhang, J. Jiang, W. L. Queen, M. R. Hudson and O. M. Yaghi, *J. Am. Chem. Soc.*, 2014, **136**, 4369–4381.